Clays and Clay Minerals, Vol. 46, No. 4, 453–465, 1998.

EFFECT OF Al AND ORGANIC ACIDS ON THE SURFACE CHEMISTRY OF KAOLINITE

DAVID B. WARD[1] AND PATRICK V. BRADY[2]

[1] Jacobs Engineering Group Inc., 2155 Louisiana Blvd. Suite 10000, Albuquerque, New Mexico 87110

[2] Geochemistry Research (MS 0750), Sandia National Laboratories, Albuquerque, New Mexico 87185

Abstract—The cause of pH and ionic strength-dependent proton and hydroxyl adsorption onto kaolinite is specific binding at edge Al and Si sites, and it can be modeled as a function of temperature with a triple layer model (TLM) of the mineral–solution interface. Exchange of Al for protons and hydroxyls is observed at low pH, with a stoichiometry approaching 1:3 ($Al:H^+$). Adsorption of organic acids from dilute solutions depends on: 1) solution pH; 2) the functionality of the acid; and, to a lesser extent, 3) temperature. Such adsorption may occur primarily at Al sites exposed on kaolinite edges, as indicated by sorption experiments on the constituent oxides, where negligible sorption was observed on SiO_2 (quartz), but was significant on Al_2O_3 (corundum) surfaces. Under similar conditions, oxalate adsorbs more strongly than acetate or formate to aluminol sites.

Key Words—Aluminum, Organic Acids, Oxalate, Surface Change.

INTRODUCTION

Interactions between clay mineral surfaces, hydroxyls and organic molecules control the geochemical cycling of a number of trace and major elements in soils and, presumably, at higher temperatures, during diagenesis. Organic acids, which are often more abundant than either protons or hydroxyls, have specifically been argued to accelerate both the dissolution (Wieland and Stumm 1992) and growth (Siffert 1962; Small 1992) of clay minerals in soils and during diagenesis. In other words, adsorbed organic acids appear to be reactive intermediates critical to the addition or removal of mineral components (Al, Si, etc.) from the bulk clay mineral phase. The mechanistic steps by which organic acids facilitate the dissolution and/or growth of silicate minerals remain unclear. This is particularly true for growth. There exists no method for predicting *a priori* 1) the extent of adsorption of a given organic ligand on a particular clay mineral surface or 2) whether the ligand will accelerate (or diminish) dissolution (or growth). Answers to each of these questions must depend on both the chemical reactivity of the various organic functional groups and on the intrinsic reactivity of the clay mineral surfaces. Generally those ligands that complex strongly with a given metal in solution also bind strongly and accelerate the corrosion of the same metal (hydr)oxide (Grandstaff 1986; Stumm et al. 1983). For silicates, the correlation between complexation, binding and corrosion is apparently more complex (Brady and House 1996). Organic ligands have been found to have less effect on dissolution rates of minerals than one might predict from aqueous speciation (Mast and Drever 1987), suggesting that crystallochemical factors deserve to be examined in further detail. On the mineral surface side, kaolinite is uniquely suited for examining multi-oxide-organic acid interactions, since 1) it contains octahedral Al_2O_3 and tetrahedral SiO_2, 2 of the primary functional groups exposed at clay surfaces; 2) it contains no easily leached cations; 3) its (hydr)oxide components exist in a variety of distinctly different structural environments (such as basal planes and edges); and 4) there is minimal substitution of variable-valence cations.

Here we first measure proton adsorption/desorption onto kaolinite (as well as quartz and corundum) and calibrate a model for kaolinite surface chemistry in organic-free solutions. We then measure the exchange of Al for surface protons. Finally, we measure adsorption of formate, acetate and oxalate onto kaolinite and use these results to examine organic anion-kaolinite surface interactions.

EXPERIMENTAL METHODS

Adsorbents

Georgia kaolinite (KGa-1; from the Source Clay Minerals Repository, University of Missouri) was used without additional pretreatment. Its specific surface area was found to be 8.58 m^2/g. Quartz (Min-U-Sil 5; from U.S. Silica, Berkeley Springs, West Virginia; crushed at Mill Creek, Oklahoma) was studied as an analog for the tetrahedral Si sites in kaolinite. It was acid-washed before use and had a specific surface area of 5.54 m^2/g. Reagent-grade α-Al_2O_3 (corundum) was obtained from Fisher Scientific for study as an analog for kaolinite's octahedral alumina sites. It was also acid-washed before was use and had a specific surface area of 0.64 m^2/g. All surface areas were measured by N_2-Brunauer-Emmett-Teller (BET) using standard methods on a Micromeritics ASAP 2000. Concomitant measurements of standards of specific surface areas similar to those of the adsorbents suggest an accuracy

of ±5% (1σ). Each adsorbent was determined by X-ray diffraction (XRD) to be mineralogically pure.

Corundum was separated from the rinse water by gravity settling, whereas centrifugation was required for the quartz powder once the pH was >3.2. Finally, the adsorbents were dried at 110 °C, driving off the last traces of HCl, and stored in air.

Potentiometric Titrations

Potentiometric titrations of suspensions of an adsorbent in NaCl electrolyte were used to infer surface charge as a function of pH by comparing the measured pH with the net concentration of acid (C_a) added (treating base as negative acid). The proton balance of such a system is:

$$C_a = [H^+] - [OH^-] + [>SOH^+_2] - [>SO^-] \quad [1]$$

where $>SOH^+_2$ and $>SO^-$ are the protonated and deprotonated surface species (see below), respectively. This may be rearranged and stated in terms of measureable parameters as:

$$\sigma_0 = C_a + \frac{K_w \times 10^{pH}}{\gamma_{OH^-}} - \frac{10^{-pH}}{\gamma_{H^+}} \quad [2]$$

where σ_0 is the net surface charge, K_w is the dissociation constant for water and γ_{H^+} and γ_{OH^-} are activity coefficients (calculated using the Davies equation (Davies 1962)).

Titrations were performed in a loosely sealed polyethylene vessel partially immersed in a constant-temperature water bath. The headspace of the vessel was continuously purged with humid Ar to exclude atmospheric CO_2. The pH was monitored by a glass combination electrode (Orion ROSS 8102), and was adjusted by addition of degassed reagents (0.1 *M* HCl and NaOH) using computer-controlled syringes with a resolution of 10^{-6} L (measurement of reagent volumes is not thought to have been a significant source of error). Temperature was monitored using a standard, Hg-filled thermometer (−20 to 110 °C, Fisher #14-983-17a) calibrated at 0 and 95 °C (the local temperature at which water boils). The pH electrode was calibrated at the temperature of interest using commercially prepared buffers (Fisher Scientific) and their reported pH values (4, 7 and 10 at 25.0 °C). Including buffer uncertainties and electrode drift, pH measurements were probably accurate to within ±0.05 or better (1σ).

To begin a series of titrations, 0.100 L of 0.001 *M* NaCl was placed in the reactor and stirred rapidly under Ar purge until its pH stabilized (usually near 6.8). Enough adsorbent was then added to give a surface concentration of 120–500 $m^2\ L^{-1}$, and was allowed to equilibrate until pH was again stable (30–90 min). Titrations then commenced with incremental addition of HCl until the lowest desired pH was reached, followed by incremental addition of NaOH until the highest desired pH was reached, and finally incremental addition of HCl again to return to the lowest desired pH. A known amount of solid NaCl was added to increase the ionic strength to ~0.1 *M*, and the NaOH and HCl titrations were repeated. Ideally, each increment of reagent would have changed the pH of the system by ~0.3 pH units. The pH was recorded when a stable reading was reached, after 1–4 min. Each "leg" of the titration required 40–90 min. Thus, only fast protonation/deprotonation reactions were measured, with little influence from the slow process that occurs over several hours (Dzombak and Morel 1990).

Reagents were calibrated with a precision of better than ±0.0003 (1 standard error, $n = 4$) *M* either by standardizing against potassium hydrogen phthalate (KHPh), or by titrating a known volume of electrolyte. In the first method, solutions containing a known amount of KHPh were titrated to an endpoint of pH 8.0, allowing the concentration of the NaOH to be calculated. In turn, the NaOH was used to neutralize a known volume of HCl, fixing its concentration as well. Volumes were measured using the same computer-controlled syringes as were used in the potentiometric titrations. In the second method, the potentiometric titration apparatus was used to measure the volumes of reagents needed to adjust the pH of 0.2 L of 0.001 *M* NaCl from 4 to 10 and back again. This was repeated 4 times, at a temperature of 25.0 °C. Reagent concentrations were calculated from mass and charge balance, using $K_w = 10^{-14}$ and activity coefficients calculated from the ion-specific extended Debye-Hückel equation. Increasing volume and ionic strength as reagents were added were also explicitly accounted for. The details of this calibration procedure may be found in Ward (1995).

Organic Anion Adsorption Measurements

Organic anion adsorption measurements were carried out in a stirred polyethylene batch reactor with inert-gas purge. Temperature control was maintained by partial immersion in a constant-temperature water bath. Adsorbents were suspended in 0.08 L of 0.01 *M* NaCl at surface concentrations of 680–1000 $m^2\ L^{-1}$ (kaolinite) or 400 $m^2\ L^{-1}$ (quartz), and the resulting suspension was spiked with an aliquot of an organic acid from a 1 g L^{-1} stock solution to give a total concentration of the organic acid added to the suspension of ~0.004–0.015 g L^{-1}. The pH was lowered to 2 by addition of HCl and then raised in increments of 0.5 to a final pH of >9 by addition of 0.1 *M* NaOH. After the pH had stabilized at each step (~1 min), an aliquot of the suspension was filtered (0.45 μm cutoff) and saved for analysis by standard high-performance liquid chromatography (HPLC) methods (Dionex Corp.) for organic anion concentration. The pH electrode was calibrated as described previously and exhibited sim-

https://doi.org/10.1346/CCMN.1998.0460410 Published online by Cambridge University Press

ilar accuracy (±0.05 or better, 1σ). HPLC measurements are thought to exhibit a precision of ±5% (1σ).

Adsorption was quantified by comparing the measured dissolved organic anion concentration with the total concentration, which was calculated from the initial composition of the system and accounting for all additions (of reagents) and withdrawals (of samples). Each of the adsorbents contained trace amounts of the organic acids of interest as well, leading to a significant blank and negative apparent adsorption values at high pH. The value of the blank contribution for each measurement series was adjusted so that calculated adsorption was zero at high pH.

Aluminum Adsorption Measurements

Aluminum adsorption/exchange by kaolinite was investigated at 25 °C (pH 3.4) and 60 °C (pH 3.5) by incrementally increasing total dissolved Al and simultaneously monitoring proton consumption. Total dissolved Al was always less than the gibbsite solubility limit determined by Wesolowski and Palmer (1992), eliminating precipitation of $Al(OH)_3$ as a possible Al sink and proton source. Measurements were performed in a stirred polyethylene batch reactor, partially immersed in a a constant-temperature bath, having restricted communication with the ambient laboratory atmosphere. A suspension of 7.2 g kaolinite in 0.2 L of 0.01 *M* NaCl was maintained at the target pH and temperature until equilibrium was reached (~90 min). Total dissolved Al was increased by adding aliquots of a 0.3 g L^{-1} Al stock solution which had been adjusted to the same pH as the suspension (because of the absence of nucleation sites, gibbsite precipitation did not occur in the stock solution on the time scale of the experiment). After Al addition, the pH was adjusted back to its target value with 0.1 *M* NaOH or HCl, as required (reagents were calibrated as described previously). Once a stable pH was achieved, the suspension was sampled for dissolved Al by filtering through a <0.45-μm filter, and the next aliquot of the Al stock solution was added. Dissolved Al was measured by DCP-AES, with a precision of ±2% (1σ) and a limit of detection of 0.0005 g L^{-1}.

Adsorption was quantified by comparing dissolved Al with total added Al, and the proton balance was calculated from the reagent volumes added. All calculated values were based on the initial composition of the system and all additions (of reagents) and withdrawals (of samples).

RESULTS

Model Development

Oxide surfaces are thought to be composed predominantly of oxygen anions that are either singly or doubly coordinated with underlying cations. The partially coordinated oxygen anions interact strongly with protons, binding them and thus neutralizing the surface's inherently negative charge. At low proton activities (high pH), oxide surfaces are typically negatively charged, and many oxygen anions will lack bound protons. At high proton activities (low pH), singly protonated oxygen anions bind additional protons, explaining observed positive surface charge. In effect, the surface oxygens are amphoteric, able to act as either a proton donor or a proton acceptor. Schematically, using >S to represent a near-surface structural cation, the neutral species >SOH can become the positively charged $>SOH^+_2$ or the negatively charged $>SO^-$. Because of its multi-oxide composition and phyllosilicate structure, kaolinite presents complexities not encountered in single oxides, with 3 distinct crystallographic surfaces. Several simplifying assumptions have been used to reduce this complexity, including: 1) edge sites dominate the complexation reactions of the surface, with negligible contributions from basal surfaces, which are dominated by either siloxane sites in silica layers or aluminol sites in gibbsite layers (Sposito 1984); 2) the N_2-BET surface area is the best available proxy for the edge surface area—the fact that BET measures total surface area contributed by all faces is offset by the observation that proton adsorption densities would otherwise be unreasonably high (Xie and Walther 1992); and 3) the edges are composed of roughly equal proportions of silanol and aluminol sites. Physically, (1) and (2) may correspond to the presence of numerous steps on the basal surfaces, effectively converting these surfaces to edges (Brady et al. 1996).

The foregoing assumptions lead to a 2-site model of the kaolinite surface, a treatment that has been developed previously using the constant capacitance model (Brady et al. 1996). The 3 important proton-surface reactions are:

$$>SiOH \rightleftarrows >SiO^- + H^+ \qquad (K^-_{Si}) \qquad [3]$$

$$>AlOH \rightleftarrows >AlO^- + H^+ \qquad (K^-_{Al}) \qquad [4]$$

$$>AlOH + H^+ \rightleftarrows >AlOH^+_2 \qquad (K^+_{Al}) \qquad [5]$$

In these equations, silanol sites are denoted by >SiOH and aluminol by >AlOH. Analogous to quartz and silica surfaces (Bolt 1957), the silanol sites on kaolinite are probably quite acidic, acting only as proton donors, whereas the aluminol sites are modeled as exhibiting amphoteric behavior. Note that proton donor/acceptor reactions can be written using fractional charges on the surface (Machesky 1990; Machesky and Jacobs 1991). We have used the stoichiometries above to model kaolinite surface charge because of their effectiveness in explaining the single oxide surface charge data (see below). The total concentration of silanol and aluminol sites is determined from the experimental conditions (specific surface area and suspended con-

https://doi.org/10.1346/CCMN.1998.0460410 Published online by Cambridge University Press

Table 1. Adjustable parameters for the triple-layer models of surface charge on quartz, corundum and kaolinite in NaCl electrolyte.

Parameter	Quartz		Corundum	Kaolinite	
	25 °C	60 °C	25 °C	25 °C	60 °C
C_1 (F/m^2)	2.20	3.15	1.1	3.8	4.9
N^s_{Si} (nm^{-2})	2.31			1.55	
N^s_{Al} (nm^{-2})			2.31	0.75	
log K^-_{Si}	−5.44	−4.68		−5.74	−5.24
log K^{Na}_{Si}	−6.93	−6.41		−6.86	−6.11
log K^-_{Al}			−10.90	−3.82	−3.97
log K^+_{Al}			6.90	4.23	4.28
log K^{Na}_{Al}			−8.22	−2.35	−1.57
log K^{Cl}_{Al}			9.58	5.50	5.69

centration of the adsorbent) and values for the site densities (N^s_{Si} and N^s_{Al}). Reasonable site densities are 1–10 nm^{-2} for simple oxides and clays (Davis and Kent 1990). To reduce the number of degrees of freedom and facilitate comparison of results, the total site density was fixed at 2.31 nm^{-2} (Davis and Kent 1990; Dzombak and Morel 1990), while allowing the silanol/aluminol ratio to vary.

The solid surface in the TLM (Davis et al. 1978; Hayes et al. 1991) is envisaged to be a charged surface to which adsorbing species are bound by chemical and electrostatic interactions (the compact or Stern layer), with charge-compensating counterions forming a diffuse layer of opposite charge in the overlying solution (the diffuse or Gouy layer). Adsorbed species, bound by chemical as well as electrostatic forces, are located in the compact layer, and may form inner-sphere complexes, in which the binding site displaces 1 of the water molecules in its inner hydration shell, or outer-sphere complexes, in which the adsorbed species retains all water molecules in its inner hydration shell. Additional counterions (both anions and cations) are distributed diffusely, maintaining the electrical neutrality of the double-layer (Hayes et al. 1991).

Many oxides develop high surface charges, as measured by potentiometric titration, but exhibit low zeta potentials, suggesting that much of the compensation of surface charge occurs in the compact layer rather than the diffuse layer. To account for this, the TLM includes reactions for specific adsorption of the electrolyte ions as outer-sphere complexes in the compact layer. For the kaolinite model presented here, 3 additional reactions are needed (for NaCl electrolyte):

$$>SiO^- + Na^+ \rightleftarrows >SiO\text{-}Na \qquad (K^{Na}_{Si}) \qquad [6]$$

$$>AlO^- + Na^+ \rightleftarrows >AlO\text{-}Na \qquad (K^{Na}_{Al}) \qquad [7]$$

$$>AlOH + H^+ + Cl^- \rightleftarrows >AlOH_2\text{-}Cl \qquad (K^{Cl}_{Al}) \qquad [8]$$

Here, the hyphen denotes an outer-sphere complex.

Three electrostatic layers are considered in the TLM: an inner (0) layer consisting of adsorbed protons and specifically adsorbed ions (inner-sphere complexes) with charge σ_0, a middle (β) layer of adsorbed electrolyte ions (outer-sphere complexes) with charge σ_β, and an outer diffuse (d) layer of counter-ions with charge σ_d. The charge-potential structure between the 0 and β planes and between the β plane and the inner edge of the diffuse layer is assumed to resemble a parallel-plate capacitor, giving rise to capacitances C_1 and C_2, respectively, while the charge-potential structure of the diffuse layer is given by Gouy-Chapman theory. Equations relating charge and potential are invariant among implementations of the TLM, and are described elsewhere (Yates et al. 1974; Davis et al. 1978; Balistrieri and Murray 1981; Davis and Kent 1990). The inner-layer capacitance (C_1) is used as a fitting parameter, whereas an outer-layer capacitance of C_2 = 0.2 F/m^2 provides good agreement between the model and measured zeta potentials on a variety of oxides (Yates et al. 1974; Davis et al. 1978).

For species adsorbing at the 0 plane (H^+ and inner-sphere complexes) on an aluminol site, their electrical potential is equated with the TLM potential ψ_0. (For outer-sphere complexes, ϕ_i is equated with ψ_β.) The intrinsic equilibrium constant for protonation of a generic surface site (K^+) is:

$$K^+_{Al} = \frac{[>AlOH_2^+]}{[>AlOH][H^+]} \times \frac{\gamma^s_{>AlOH_2^+}}{\gamma^s_{>AlOH}\gamma_{H^+}} \times e^{(\psi_0)F/RT} \qquad [9]$$

Based on the arguments of Chan et al. (1975), it is assumed that the activity coefficients of surface species depend only on the properties of the electrical double-layer and not on the charges of the individual sites; thus $\gamma^s_{>AlOH2}^+$ and $\gamma^s_{>AlOH2}^+$ cancel one another, giving rise to:

$$K^+_{Al} = \frac{[>AlOH_2^+]}{[>AlOH][H^+]} \times \frac{1}{\gamma_{H^+}} \times e^{(\psi_0)F/RT} \qquad [10]$$

$$K^-_{Si} = \frac{[>SiO^-][H^+]}{[>SiOH]} \times \gamma_{H^+} \times e^{(-\psi_0)F/RT} \qquad [11]$$

$$K^-_{Al} = \frac{[>AlO^-][H^+]}{[>AlOH]} \times \gamma_{H^+} \times e^{(-\psi_0)F/RT} \qquad [12]$$

$$K^{Na}_{Si} = \frac{[>SiO\text{-}Na][H^+]}{[>SiOH][Na^+]} \times \frac{\gamma_{H^+}}{\gamma_{Na^+}} \times e^{(\psi_\beta-\psi_0)F/RT} \qquad [13]$$

$$K^{Na}_{Al} = \frac{[>AlO\text{-}Na][H^+]}{[>AlOH][Na^+]} \times \frac{\gamma_{H^+}}{\gamma_{Na^+}} \times e^{(\psi_\beta-\psi_0)F/RT} \qquad [14]$$

$$K^{Cl}_{Al} = \frac{[>AlOH_2\text{-}Cl]}{[>AlOH][H^+][Cl^-]} \times \frac{1}{\gamma_{H^+}\gamma_{Cl^-}} \times e^{(\psi_0-\psi_\beta)F/RT} \qquad [15]$$

The remaining parameters needed to specify the TLM are listed in Table 1, along with their measured values for quartz, corundum and kaolinite. These were used as adjustable parameters and were found using the nonlinear least-squares optimization program FI-

https://doi.org/10.1346/CCMN.1998.0460410 Published online by Cambridge University Press

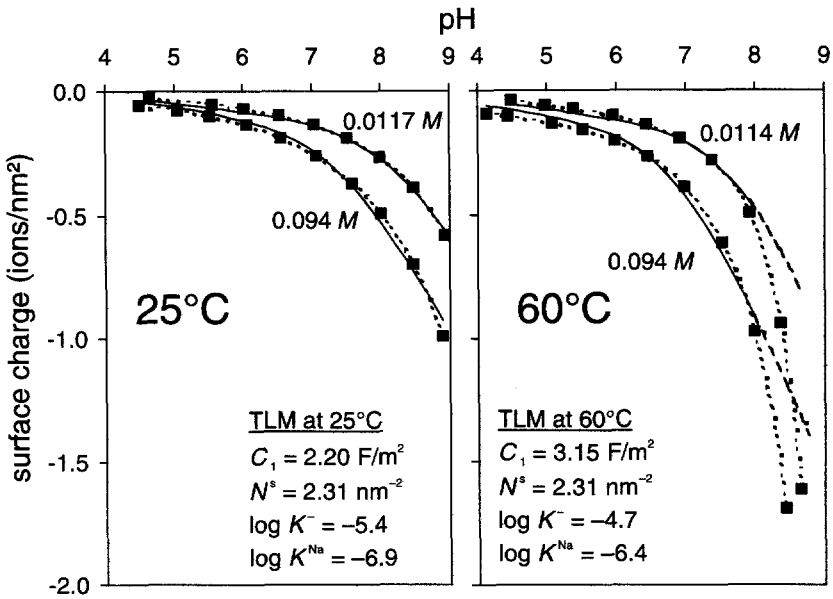

Figure 1. Potentiometric titrations and TLM for surface charge on quartz at 25 and 60 °C.

TEQL 3.0 (Herbelin and Westall 1994) to minimize the variance between measured and calculated potentiometric titration curves. Titrations at 2 different ionic strengths (3 for corundum) were regressed simultaneously in order to better constrain the role of the outer-sphere electrolyte complexes. Input to FITEQL was calculated using the temperature-corrected Davies equation, but internal calculations always used activity corrections for 25 °C, slightly overestimating activity coefficients at higher temperatures. The dissociation constant for water was taken to be log $K_w = -14$ at 25 °C and −13.00 at 60 °C (Stumm and Morgan 1981).

Experimentally determined values were assigned uncertainties using FITEQL's default 1σ values, that is, pH precision was ±0.01, and errors in total H^+ were the greater of ±1% or 1×10^{-6} *M*. The precision of individual pH measurements is much better than this, but drift and the accuracy of the electrode calibration must also be accounted for, so this precision is a reasonable estimate. Likewise, the precision of each increment of acid or base added to adjust total H^+ is also more precise than modeled, but accuracy of reagent calibration and cumulative pipetting errors must also be considered. These error estimates result in a goodness-of-fit statistic, *F* (called WSOS/DY in FITEQL), of ~50 or better for models that visually appear to adequately describe the potentiometric titration measurements.

Because surface charge on kaolinite is due to protonation and deprotonation reactions at sites with either Si^{4+} in tetrahedral coordination or Al^{3+} in octahedral coordination as the metal cation, some insights into the behavior of these sites may be gained by examining simple oxides in which the cation shows the same coordination. Quartz (α-SiO_2) provides an analog for the silica sites, and corundum (α-Al_2O_3) is used for the alumina sites.

Surface charge measurements and model results for quartz are shown in Figure 1. The site density was fixed at $N^s_{Si} = 2.31$ nm^{-2}, and FITEQL was used to optimize K^-_{Si} and K^{Na}_{Si}. At 60 °C, titration data above pH 8 were excluded from the model, limiting model applicability to pH values below this. The significance of the high surface charge observed at greater pH values has not been assessed, but may indicate increased quartz solubility and increased deprotonation of H_4SiO_4 to $H_3SiO^-_4$. Blank titrations indicate essentially linear electrode response up to pH 10 at 25 °C and pH 9 at 60 °C, ruling out measurement inconsistencies. At 25 °C, the values for K^-_{Si} and K^{Na}_{Si} are similar to those that have been reported previously (Hayes et al. 1990) and serve as a validation of the potentiometric titration method employed here. Quartz has a low pH_{ZPC} near 2 (compare Bolt 1957) but becomes deprotonated only when conditions are comparatively basic. In other words, it is very slow to develop surface charge as pH is increased, as reflected by the small values of K^-_{Si} and K^{Na}_{Si} compared to the pH_{ZPC}. This is important for correlating site behavior with cation identity on kaolinite.

Temperature Effects

Increasing temperature leads to increasingly negative surface charge at a given pH, reflected in the increasing magnitude of the deprotonation and Na-complexation equilibrium constants (K^-_{Si} and K^{Na}_{Si}, re-

https://doi.org/10.1346/CCMN.1998.0460410 Published online by Cambridge University Press

Table 2. Enthalpy, Gibbs' free energy and entropy for surface-complexation reactions.

Equilibrium constant	ΔH (kJ mol^{-1})	$\Delta G^{\circ}_{25°C}$ (kJ mol^{-1})	ΔS° (J mol^{-1} K^{-1})
Quartz			
K^{-}_{Si}	41.30	31.06	34.4
K^{Na}_{Si}	28.26	39.56	−37.9
Alumina			
Single-K model	53.25	−53.95	359.6
Kaolinite			
K^{-}_{Si}	27.17	32.77	−18.8
K^{Na}_{Si}	40.76	39.16	−5.3
K^{-}_{Al}	−8.15	21.81	−100.5
K^{+}_{Al}	2.72	−24.15	90.1
K^{Na}_{Al}	42.39	13.42	−97.2
K^{Cl}_{Al}	10.32	−31.40	139.9

spectively). Application of the integrated Van't Hoff equation:

$$\Delta H = R \ln\left(\frac{K_2}{K_1}\right) \times \left(\frac{1}{T_1} - \frac{1}{T_2}\right)^{-1} \quad [16]$$

allows the enthalpy change of each reaction to be calculated. The standard state Gibbs free energy change may be calculated from the equilibrium constants ($\Delta G^{\circ} = -RT \ln K$, at the pH_{ZPC} where electrostatic terms approach zero), permitting estimation of the change in entropy ($\Delta S^{\circ} = (\Delta H - \Delta G^{\circ})/T$), both of which are assumed to be constant over the temperature range 25–60 °C. ΔH, $\Delta G^{\circ}_{25\,°C}$, and ΔS are compiled in Table 2. Proton loss is endothermic, but the subsequent step of adsorbing Na as an outer-sphere complex is exothermic, as shown by the smaller ΔH for the Na-exchange reaction compared to deprotonation. Similarly, deprotonation is accompanied by a significant increase in entropy, but Na adsorption produces a much larger decrease in entropy.

The modeled capacitance of the interface also increases with temperature, changing from 2.20 to 3.15 F/m^2 as T changes from 25 to 60 °C. This is counterintuitive, because the dielectric constant for water decreases with temperature, from 78 at 25 °C to 67 at 60 °C (Weast 1973). If temperature has a similar effect on the structured water of the mineral-solution interface, then the model assumptions of constant surface area and site density may be erroneous.

Surface charge on corundum was modeled using the measurements of Hayes et al. (1990) at 25 °C on an acid-washed powder with a specific surface area of 12.6 m^2/g Hayes et al. (1991). Results are shown in Figure 2. The model was constructed following the recommendations of Hayes et al. (1991), fixing K^{-}_{Al} at $10^{-10.90}$ and K^{+}_{Al} at $10^{6.90}$, for $pH_{ZPC} = 8.90$ ($pH_{ZPC} = 0.5(pK^{-}_{Al} - pK^{+}_{Al})$). To be consistent with the quartz model, the site density was fixed at 2.31 nm^{-2}. The inner-layer capacitance, C_1, was optimized manually while FITEQL was used to optimize the electrolyte-binding constants, K^{Na}_{Al} and K^{Cl}_{Al}. The resulting fit is excellent ($F = 10.1$), deviating from the measurements significantly only at pH < 9.5, where the buffering capacity of water begins to become significant. The fact that the 0.005- and 0.030-M curves cross at high pH suggests that these measurements may contain some systematic deviations.

The TLM for corundum sharply contrasts with the quartz TLM. Using the pH_{ZPC} as a point of reference, it is apparent that surface charge develops much more quickly on corundum as the pH deviates from the pH_{ZPC}. This is manifest in the corundum TLM as small values for $\Delta pK^{H^+}_{Al}$ ($\equiv pK^{-}_{Al} + pK^{+}_{Al}$) and $\Delta pK^{electrolyte}_{Al}$ ($\equiv pK^{Na}_{Al} + pK^{Cl}_{Al}$); for quartz these values are so large that the positively charged surface species can be omitted from the model without compromising it. Additionally, the corundum interface has a somewhat lower capacitance than quartz ($C_1 = 1.10$ vs. 2.20 F/

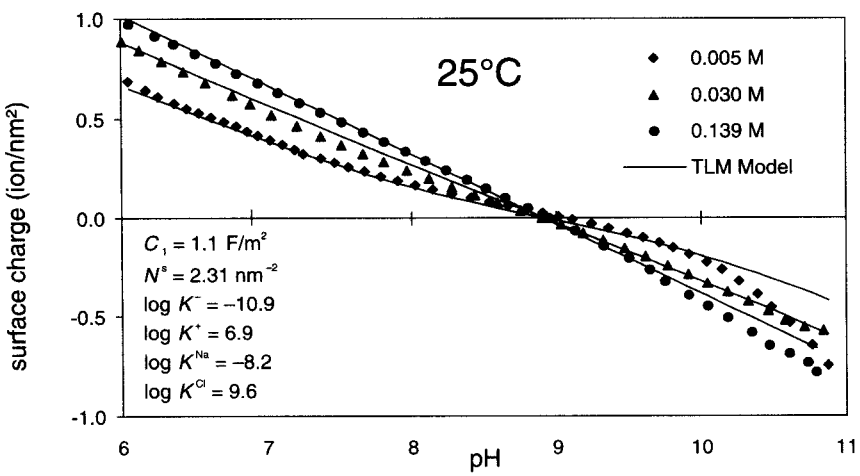

Figure 2. TLM for surface charge on corundum (α-Al_2O_3) at 25 °C using measurements of Hayes et al. (1990).

https://doi.org/10.1346/CCMN.1998.0460410 Published online by Cambridge University Press

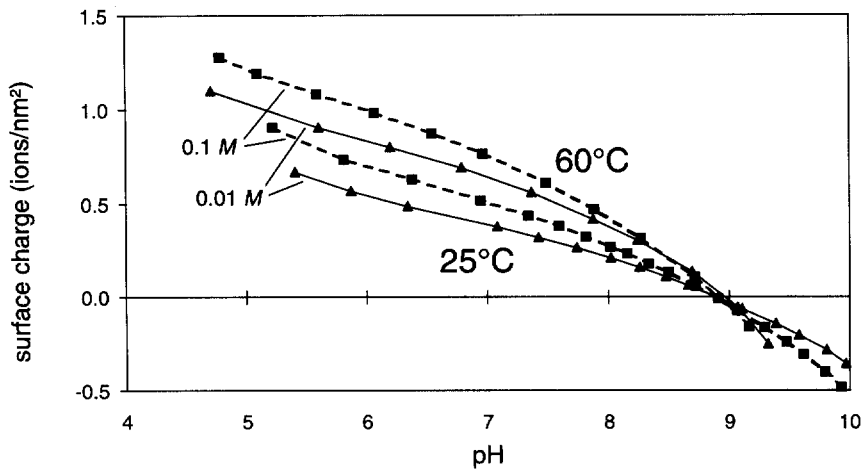

Figure 3. Temperature dependence of surface charge on corundum (α-Al_2O_3) at 25 and 60 °C.

m^2). It thus develops a greater potential for a given charge, accentuating the electrostatic role of the mineral solution interface.

The temperature-dependence of proton equilibria of the corundum surface is illustrated by potentiometric titration measurements at 25 and 60 °C made as part of this study, shown in Figure 3. These curves are not amenable to description using the TLM because they are everywhere concave downward, lacking an inflection at the pH_{ZPC}. Additionally, the pH of intersection of the two 60 °C curves is quite uncertain because of the small angle at which they cross. Here the pH of intersection was adjusted during data reduction to match the 25 °C data by adding a constant offset in total H^+ to the 0.1-*M* measurements. This juxtaposition implies that temperature must similarly affect both the protonation and deprotonation reactions, leaving the pH_{ZPC} unaltered. If this is true, then the greater magnitude surface charge observed at higher temperature implies that both the protonation and the deprotonation reactions are endothermic.

This is at odds with the literature survey by Machesky (1990), who extracted enthalpies of adsorption near −40 kJ mol^{-1} from several studies of alumina protonation (Tewari and McLean 1972; Van Den Vlekkert et al. 1988; Machesky and Jacobs 1991) using a simple single-*K* model without electrolyte binding or electrical double-layer effects: $>SO^{-1/2} + H^+ \rightleftharpoons >SOH^{+1/2}$. The single-*K* model may be evaluated for the current data set by extrapolating from the linear portions of the curves (at pH < 7) to zero surface charge, at which point log *K* = pH (that is, pH 9.45 and 10.43 for 25 and 60 °C, respectively). These *K* values may then be used in the van't Hoff equation to calculate ΔH, giving an exothermic value of 53.25 kJ mol^{-1}. Because of the extrapolation from pH < 7 where the concentration of $>AlO^-$ is negligible in comparison with >AlOH and $>AlOH^+_2$, this enthalpy change may loosely correlate with the sum of reactions for K^+_{Al} of Equation [5] and K^{Cl}_{Al} of Equation [8].

A Surface Complexation Model for Kaolinite

Potentiometric titration measurements for kaolinite at 25 and 60 °C are presented in Figure 4, along with TLM curves for the 2-site model. The model was developed using the 25 °C measurements and the quartz *K* values for the silica sites. For the alumina sites, ΔpK^{H+}_{Al} was set to zero at a pH_{ZPC} of 4 (log K^+_{Al} = −log K^-_{Al} = 4). The site densities and K^{Na}_{Al} were specified as fitting parameters in FITEQL, and the inner-layer capacitance, C_1, was varied manually until N^s_{Si} + N^s_{Al} = ~2.31 nm^{-2}. This process was repeated (with fixed C_1) for K^+_{Al}, K^-_{Al} and K^{Cl}_{Al}. Site densities were than held constant, and K^-_{Si} and K^{Na}_{Si} were optimized. Finally, each alumina *K* was optimized alone. At this point, changes in each log *K* were small (<0.01), so fitting was complete. Visually, there are discrepancies between the measured and modeled surface charge, but they are of minor significance, as reflected by the reasonably low values of *F* (20.9 and 26.1 at 25 and 60 °C, respectively). This TLM successfully reproduces the important features of the surface charge patterns as a function of both ionic strength and temperature.

Speciation at the kaolinite : solution interface as calculated using this TLM is presented in Figure 5. The silica sites remain neutral until pH > 7, at which point they begin to significantly deprotonate. At higher ionic strength and temperature, the outer-sphere Na complex, >SiO-Na, becomes increasingly stable. This behavior is reminiscent of silica sites on quartz, with only slight variations in the relative magnitudes of K^-_{Si} and K^{Na}_{Si} (not surprising because these values were the last to be varied during the modeling procedure). The alumina sites in kaolinite are much different from those in corundum, however. Most striking is the shift in pH_{ZPC} from 8.90 to ~4. Apparently, the proximity

https://doi.org/10.1346/CCMN.1998.0460410 Published online by Cambridge University Press

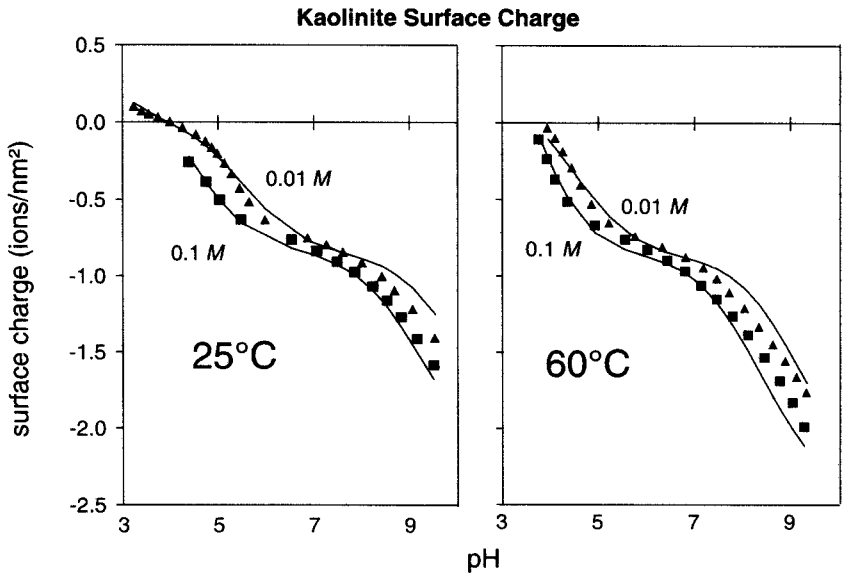

Figure 4. Potentiometric titrations and TLM for surface charge on kaolinite at 25 and 60 °C.

of the very acidic silica sites, with electron density shifted from the O^{2-} anions towards the central Si^{4+} cations, perturbs the electron density around the O^{2-} ions of the alumina sites as well. The ΔpK^{H+}_{Al} for the alumina sites is approximately −0.4 instead of 4, indicating much greater stability of the protonated and deprotonated species relative to the neutral species than was found for corundum. This is required by the TLM in order to reproduce the sharp bends in the surface charge curve between pH 4 and 6. Simpler surface complexation models (such as the diffuse-layer model or the constant capacitance model) lack the screening effect of the outer-sphere complexes, so are able to produce much sharper changes in abundance of surface species, more closely resembling trends for purely aqueous species. For kaolinite, the strength of the >AlO-Na complex is much greater than for corundum. This is also a consequence of parameterizing the TLM model to reproduce the sharp bends in the surface-charge curve. In the TLM model presented here, the plateau at pH 6–7 reflects the nearly complete deprotonation of the alumina sites before the pH is high enough to significantly deprotonate the silica sites. This is accomplished by assigning comparatively large equilibrium constants to $>AlO^-$ and >AlO-Na. Finally, the capacitance of the interface (C_1) is much higher for kaolinite than for corundum (3.8 vs. 1.1 F/m² at 25 °C). Because of the tradeoff between site

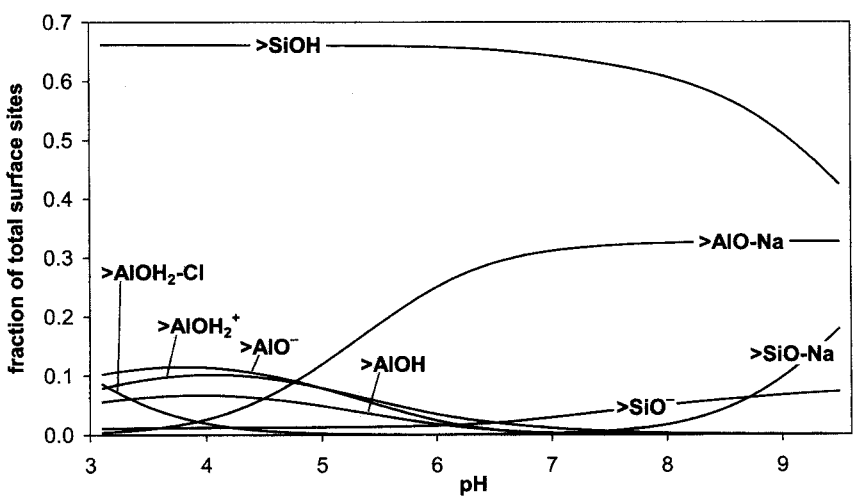

Figure 5. Calculated speciation of the kaolinite surface in 0.01 *M* NaCl at 25 °C.

https://doi.org/10.1346/CCMN.1998.0460410 Published online by Cambridge University Press

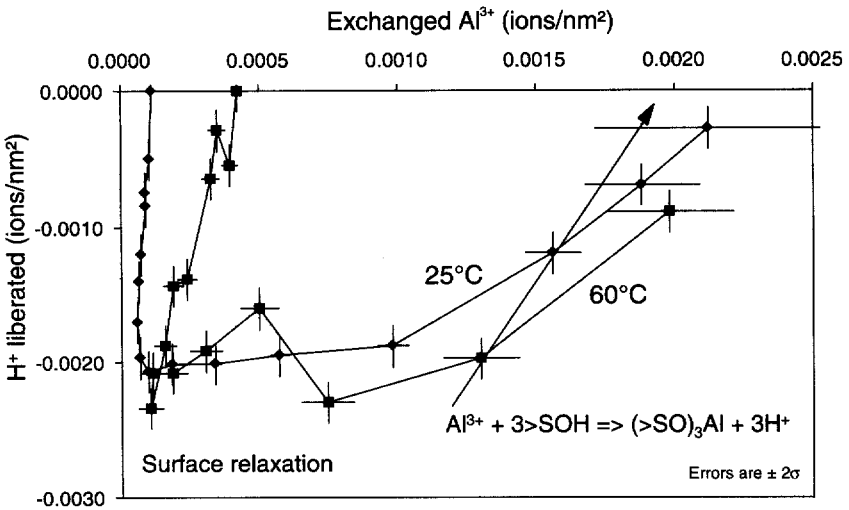

Figure 6. Adsorption of Al by kaolinite at 25 and 60 °C in 0.01 *M* NaCl at low pH.

density and capacitance, this may imply that the actual site density is higher than modeled, or it may reflect a peculiarity of the edge-site geometry and the presence of numerous steps on the kaolinite basal surfaces (Brady et al. 1996).

The ratio of silica to alumina sites is substantially greater than the 1:1 ratio suggested by the stoichiometry of the kaolinite unit cell for edge sites. This may be a modeling artifact, or possibly the result of *in-situ* partial dissolution at near-neutral pH values, where the alumina sites are largely deprotonated and hence easily dissolved in comparison to the nearly neutral silica sites. The model cannot differentiate between the two. The effect of temperature on the kaolinite/electrolyte interface is dominated by the unusually endothermic character of the >AlO-Na exchange reaction, and at high pH by >SiO-Na, reflected by the large ΔH values (compare Table 2) and greater stability of these complexes at higher temperature (compare Figure 5). The calculated entropic effects are at odds with chemical intuition, particularly for the formation of $>AlOH_2$-Cl, which shows a positive ΔS, whereas one would expect $\Delta S < 0$ due to the ordering effect of confining hydrated Cl^- and an additional proton to surface sites. Similarly, one would expect ΔS for $>AlO^-$ to be >0 because a proton is liberated to the solution, whereas the modeled value is <0. These unusual features suggest that the mechanistic implications of the TLM should not be interpreted too literally. Nevertheless, this model is an improvement over the constant-capacitance and diffuse-layer surface-complexation approaches, reasonably accounting for the effects of ionic strength. It may be possible to further validate the TLM by measuring zeta potentials as a function of ionic strength and comparing them with the calculated potentials at the inner edge of the diffuse layer (ψ_β), which has been tentatively correlated with the shear plane between a moving particle and the bulk solution.

Al Exchange on Kaolinite

A necessary step to formulating a model for kaolinite surface chemistry, as well as dissolution and growth (Oelkers et al. 1994), is to measure the affinity of the surface for its components, Si and Al. We focus on the latter. An attempt was made to determine the stoichiometry of Al^{3+}-H^+ exchange by measuring proton release as Al^{3+} was added to a suspension of kaolinite at constant pH. Such measurements are complicated by the limited solubility of Al at near-neutral pH (Wesolowski and Palmer, 1992), and the low affinity of the kaolinite surface for Al^{3+} at lower pH due to unfavorable electrostatic interactions between the neutral or positively charged surface and the Al cation. Attempting such measurements at high pH faces similar difficulties, because Al in solution occurs predominantly as the hydroxy complex $Al(OH)^-_4$, which would face unfavorable electrostatic interactions with the highly negatively charged kaolinite surface. Nevertheless, measurements made at 25 °C (pH 3.40) and 60 °C (pH 3.50) were able to resolve some exchange of H^+ for Al^{3+}, as shown in Figure 6. Maximum dissolved Al was 104×10^{-6} *M* at 25 °C (23% of total Al was adsorbed) and 57×10^{-6} *M* at 60 °C (34% of total Al was adsorbed), below saturation with respect to gibbsite. The results are complicated by the extensive "surface relaxation" that consumed H^+ during the early part of the experiment with little change in the quantity of adsorbed Al^{3+} even as dissolved Al^{3+} was being slowly increased. As progressively greater amounts of Al^{3+} were added to the system, Al exchange gradually became the dominant reaction, leading to increasing amounts of liberated H^+. One pos-

https://doi.org/10.1346/CCMN.1998.0460410 Published online by Cambridge University Press

Table 3. Dissociation constants of formic, acetic and oxalic acids.

Organic acid	T (°C)	pK_{a_1}	pK_{a_2}
Formic†	20	3.75	—
	25	4.77	—
Acetic‡	60	4.76	
Oxalic§	25	1.28	4.28
	60	1.40	4.47

† Weast (1973).
‡ Bethke (1994).
§ Kettler et al. (1991).

tulated exchange reaction at the kaolinite surface is (Oelkers et al. 1994):

$$Al^{3+} + 3{>}SOH \rightleftarrows (>SO)_3Al + 3H^+ \quad [17]$$

whose trajectory is illustrated by the upward-pointing solid arrow in Figure 6. The slope of the experimental measurements is somewhat shallower than, but reasonably consistent with, the value of 3 required by this reaction, as "surface relaxation" processes were undoubtedly still contributing to the proton balance of the system (the latter would be forcing the slope to be less than 3).

Oxalate and Acetate and Formate Adsorption on Quartz and Kaolinite

Fractional adsorption as a function of pH was measured for the monodentate acetic and formic acids (CH_3COOH and HCOOH), and for the bidentate oxalic acid (HOOCCOOH), at 25 and 60 °C in 0.01 *M* NaCl for kaolinite and quartz. Dissociation constants for these acids are listed in Table 3. Results for acetate and formate are shown in Figure 7. Neither anion was significantly adsorbed by quartz at any pH, and kaolinite showed only slight affinity for acetate and formate (<10% adsorbed) for pH <6. Oxalate is also only weakly adsorbed by quartz (<5% at pH <6), but shows a much stronger affinity for kaolinite, reaching 80% adsorbed at pH 5.5 (25 °C) with a broad adsorption edge from pH 9 down to 6 (Figure 8). Below pH 5.5, adsorption declines somewhat to 65% at pH 3.5, before climbing again to >70% at pH 2. At 60 °C, the curve is shifted towards lower pH, and shows a slightly greater maximum adsorption.

A quantitative triple-layer model for oxalate adsorption on kaolinite is illustrated in Figure 8. The previously developed surface-charge TLM provided the basis for the adsorption model. Additional aqueous species were included for oxalate (Ox^{2-}) protonation:

$$Ox^{2-} + H^+ \rightleftarrows HOx^- \qquad \log K_{HOx^-} = -pK_{a_2} \quad [18]$$

$$Ox^{2-} + 2H^+ \rightleftarrows H_2Ox \qquad \log K_{H_2Ox} = -(pK_{a_1} + pK_{a_2}) \quad [19]$$

The quartz data indicate that oxalate does not interact with silica sites, and Fein and Brady (1995) showed that oxalate adsorbs strongly to alumina sites at low pH, with an adsorption edge near pH 9.5 (γ-Al_2O_3, oxalate : alumina sites = ~0.02, assuming 2.31 sites/nm^2). Thus the alumina sites are assumed to be the locus of oxalate adsorption on kaolinite. In the kaolinite experiments, the oxalate : aluminol ratio was ~0.2, but the lack of complete adsorption at low pH indicates that the available adsorption sites were saturated. This was incorporated into the TLM by distributing the aluminol sites among 2 subpopulations based on whether or not they interacted with oxalate. The fraction of aluminol sites interacting with oxalate, denoted by X^{Ox}_{Al}, was adjusted manually to obtain the best fit to the experimental measurements. The behavior of each subpopulation with respect to protons and the background electrolyte was indentical.

Numerous possible stoichiometries for the oxalate surface complex were examined, but most predicted a very steep adsorption edge, with a transition width of only 1 pH unit or so. Better results were obtained with a somewhat unorthodox complex consisting of deprotonated oxalate bound to a neutral aluminol in an outer-sphere configuration, which produced a transition width of ~2 pH units, nearly as broad as measured. Conceptually, we intepret this monodentate complex to resemble hydrogen bonding between oxalate and the surface. The equilibrium expression used in the TLM for this reaction is:

$$K^{Ox}_{Al} = \frac{[{>}AlOH\text{-}Ox^{2-}]}{[{>}AlOH][Ox^{2-}]} \times \frac{\gamma_{>-Ox^-}}{\gamma_{Ox^{2-}}} \times e^{(-\psi_\beta)F/RT} \quad [20]$$

where $\gamma_{>-Ox^-}$ is the activity coefficient for the uncomplexed carboxylate group in the bound oxalate, and $\gamma_{Ox^{2-}}$ is the activity coefficient for dissolved oxalate. Fitting was accomplished at each temperature by letting FITEQL optimize K^{Ox}_{Al} to obtain the best fit for a given value of X^{Ox}_{Al} for all measurements across the adsorption edge (that is, for pH > pH of maximum adsorption).

The model suggests that the enthalpy of adsorption is low, as shown by the nearly identical values of K^{Ox}_{Al} at 25 and 60 °C. The major factor causing the adsorption edge to shift toward lower pH by more than 0.5 pH units is the greater negative surface charge at the higher temperature. This TLM explains the overall trend observed for oxalate adsorption on kaolinite, but does not reproduce the decline in adsorption seen below pH 5 or the very shallow slope of the adsorption edge observed at 25 °C. The difficulties at pH 5 suggest that the TLM may not present a complete description of complexation at the kaolinite : solution interface—in order to produce a peak at pH 5, the kaolinite TLM would have to exhibit a rapid change in speciation and surface charge at this pH, much like that exhibited at the pH_{ZPC} (that is, pH 4; compare Figure

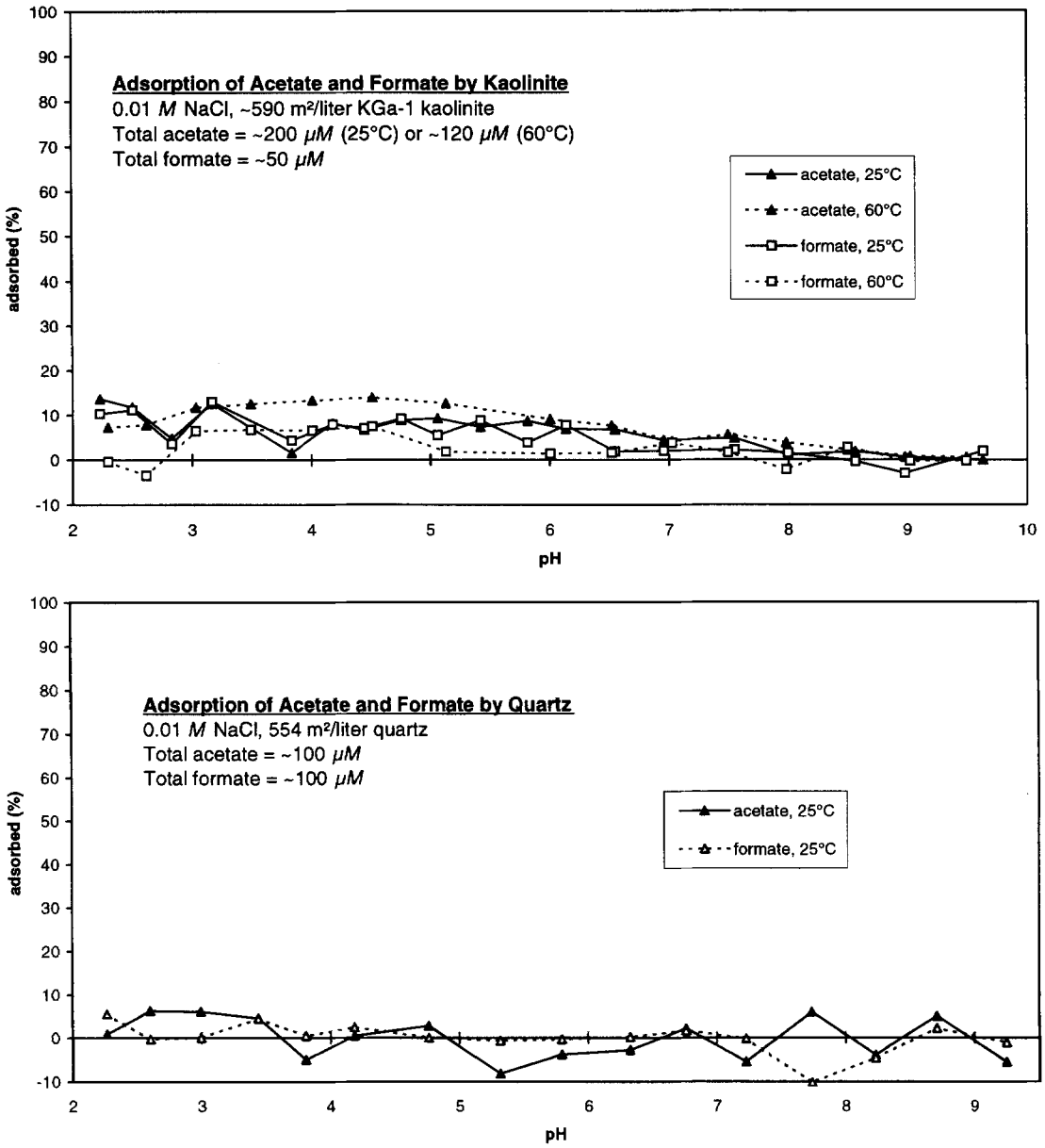

Figure 7. Adsorption of acetate and formate in 0.01 *M* NaCl by quartz and kaolinite.

5). Indeed, for small values of their equilibrium constants, several hypothetical oxalate surface complexes produced adsorption peaks rather than edges, but these were approximately symmetrical about the model's pH_{ZPC}. It seems unlikely that the presence of oxalate could so drastically shift the pH_{ZPC} of kaolinite here. Another possibility may be the influence of Al-oxalate complexes in solution, but this seems unlikely. Although dissolved Al was not monitored, calculations assuming gibbsite saturation offered little improvement. Additionally, the Al-exchange experiments argue that the amount of kaolinite dissolution is minimal during the time scale of these measurements.

A key assumption in the TLM is that each type of adsorption site is identical, when in fact a collection of sites exhibits a continuum of affinities due to variations in the local geometry of each site (Dzombak and Morel 1990). In cases where only a small fraction of the total sites are occupied by the adsorbent of interest, only the highest-affinity sites are occupied, and the uniform-site approximation provides a good description of the adsorption curve. Here, however, ox-

https://doi.org/10.1346/CCMN.1998.0460410 Published online by Cambridge University Press

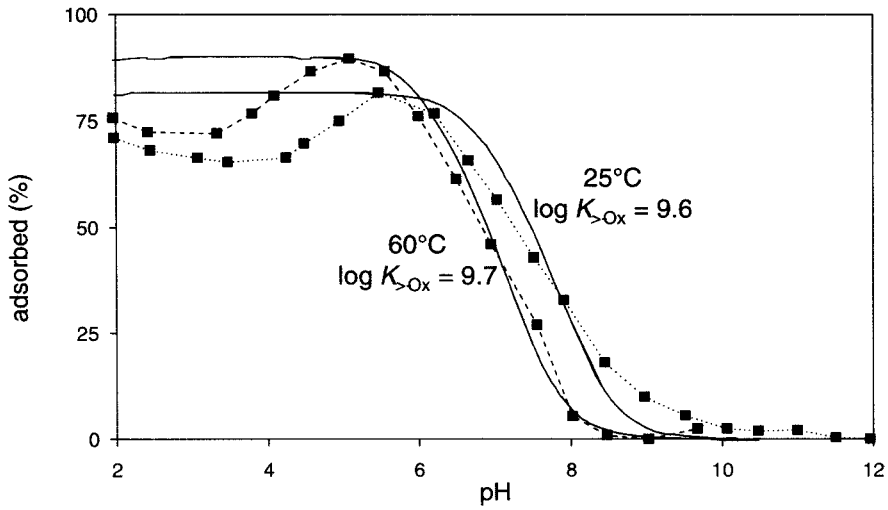

Figure 8. Adsorption of oxalate on kaolinite at 25 and 60 °C in 0.01 *M* NaCl and TLM fit for oxalate adsorption.

alate has saturated the available sites, occupying the highest-affinity sites first at high pH and progressing to less favorable sites at lower pH as electrostatic interactions become more favorable. Thus, the slope of the measured adsorption edge is shallower than predicted by the TLM. To be more realistic, the equilibrium "constant" describing adsorption measured in bulk should actually be a function of pH, declining with declining pH.

CONCLUSIONS

The major points to be drawn from our work are:

1) The pH-dependent kaolinite surface charge can be reasonably well represented with a TLM; organic acid adsorption less so.

2) Oxalate sorbs at near and less than neutral pH. We hypothesize that interaction between oxalate and the kaolinite surface occurs primarily at exposed Al sites. Oxalate sorbs much more strongly than acetate and formate.

3) Al appears to exchange 1:3 for protons at less than neutral pH and 1:4 with OH at high pH.

ACKNOWLEDGMENTS

We greatly appreciate funding from DOE/BES-Geosciences and NRC, 2 constructive reviews from anonymous reviewers and helpful discussions with E. Oelkers and J. Schott. This work was supported by the U.S. Department of Energy under Contract DE-AC 04-94 AL 85000.

REFERENCES

Balistrieri LS, Murray JW. 1981. The surface chemistry of goethite (alpha FeOOH) in major ion seawater Am J Sci 281:788–806.

Bethke CM. 1994. The geochemist's workbench™. A users guide to Rxn, Act2, Tact, React, and Gtplot. Champaign, IL: Univ of Illinois. 212 p.

Bolt G. 1957. Determination of the charge density of silica sols J Phys Chem 61:1166–1170.

Brady PV, Cygan RT, Nagy KL. 1996. Molecular controls on kaolinite surface charge. J Coll Interf Sci 183:356–364.

Brady PV, House WA. 1996. Surface-controlled dissolution and growth of minerals. In: Brady PV, editor. Physics and chemistry of mineral surfaces. Boca Raton, FL: CRC Pr. p 225–306.

Chan D, Perram JW, White LW. 1975. Regulation of surface potential at amphoteric surfaces during particle-particle interaction. J Chem Soc, Faraday Trans 71:1046–1057.

Davies CW. 1962. Ion association. Washington, DC: Butterworth. 180 p.

Davis JA, James RO, Leckie JO. 1978. Surface ionization and complexation at the oxide-water interface. 1. Computation of electrical double layer properties in simple electrolytes. J Colloid Interface Sci 63:480–499.

Davis JA, Kent DB. 1990. Surface complexation modeling in aqueous chemistry. In: Hochella MF, White AF, editors. Mineral-interface geochemistry. Washington, DC: Am Mineral Soc. p 177–260.

Dzombak DA, Morel FMM. 1990. Surface complexation modeling: Hydrous ferric oxide. New York: J. Wiley. 393 p.

Grandstaff DE. 1986. The dissolution rate of forsteritic olivine from Hawaiian beach sand. 3rd Int Water-Rock Interaction Symp. Geochem and Cosmochem Soc, Alberta Research Council. p 72–74.

Hayes KF, Redden GW, Leckie JO. 1990. Application of surface complexation models for radionuclide adsorption: Sensitivity analysis of model input parameters final report. Washington, DC: USNRC. 72 p.

Hayes KF, Redden GW, Leckie JO. 1991. Surface complexation models: An evaluation of model parameter estimation using FITEQL and oxide mineral titration data J Colloid Interface Sci 142:448–469.

Herbelin AL, Westall JC. 1994. FITEQL—A computer program for determination of chemical equilibrium constants from experimental data. Oregon State Univ Chem Dept.

Kettler RM, Palmer DA, Wesolowski DJ. 1991. Dissociation quotients of oxalic acid in aqueous sodium-chloride media to 175 degrees C. J Solution Chem 20:905–927.

Machesky ML. 1990. Influence of temperature on ion adsorption by hydrous metal oxides. In: Melchior DC, Bassett RL, editors. Chemical modeling in aqueous systems II.

ACS Symp Series #416. Washington, DC: ACS. p 262–274.

Machesky ML, Jacobs PF. 1991. Titration calorimetry of aqueous alumina suspensions, Part II. Discussion of enthalpy changes with pH and ionic strength. Colloids and Surf 53:315–328.

Mast MA, Drever JI. 1987. The effect of oxalate on the dissolution rates of oligoclase and tremolite. Geochim Cosmochim Acta 51:2559–2568.

Oelkers EH, Schott J, Devidal JL. 1994. The effect of aluminum, pH, and chemical affinity on the rates of aluminosilicate dissolution reactions. Geochim Cosmochim Acta 58:2011–2024.

Siffert B. 1962. Quelques reactions de la silice en solution: La formation des argiles. Mem Serv Carte Geol 21:1–86.

Small JS. 1992. Clay precipitation from oxalate-bearing solutions. In: Kharaka Y, Maest AS, editors. Water-rock interaction. Rotterdam: Balkema. p 345–348.

Sposito G. 1984. The surface chemistry of soils. New York: Oxford Univ Pr. 234 p.

Stumm W, Furrer G, Kunz B. 1983. The role of surface coordination in precipitation and dissolution of mineral phases. Croat Chim Acta 46:593–611.

Stumm W, Morgan JJ. 1981. Aquatic chemistry. New York: Wiley-Interscience. 780 p.

Tewari PH, McLean AW. 1972. Temperature dependence of point of zero charge of alumina and magnetite. J Colloid Interface Sci 40:267–272.

Van Den Vlekkert H, Bousse L, de Rooij N. 1988. The temperature dependence of the surface potential at the Al2O3/electrolyte interface. J Colloid Interface Sci 122:336–345.

Ward DB. 1995. Nickel adsorption on a natural sand and goethite, kaolinite, and quartz: Single- vs. multi-site models and the role of CO2. Albuquerque, NM: Univ of New Mexico. 304 p.

Weast RC. 1973. Handbook of chemistry and physics, 61st edition. Boca Raton, FL: CRC Pr. 2488 p.

Wesolowski DJ, Palmer DA. 1992. Aluminum speciation and equilibria in aqueous solution: V. Gibbsite solubility at 50°C and pH 3–9 in 0.1 molal NaCl solutions. Geochim Cosmochim Acta 58:2947–2969.

Wieland E, Stumm W. 1992. Dissolution kinetics of kaolinite in acidic aqueous solutions at 25 °C. Geochim Cosmochim Acta 56:3339–3355.

Xie Z, Walther JV. 1992. Incongruent dissolution and surface area of kaolinite. Geochim Cosmochim Acta 56:3357–3363.

Yates DE, Levine S, Healy TW. 1974. Site-binding model of the electrical double layer at the oxide/water interface. J Chem Soc London, Faraday Trans 70:1807–1818.

(Received 7 November 1996; accepted 10 November 1997; Ms. 2828)